ACS APPLIED MATERIALS & INTERFACES

Research Article

www.acsami.org

SERS Detection of Amyloid Oligomers on Metallorganic-Decorated Plasmonic Beads

Luca Guerrini,[†,‡] Raul Arenal,[§,∥] Benedetta Mannini,[⊥] Fabrizio Chiti,[⊥] Roberto Pini,[#] Paolo Matteini,*[,#] and Ramon A. Alvarez-Puebla*[,†,‡,○]

[†]Universitat Rovira i Virgili and Centro de Tecnologia Quimica de Cataluña, C/de Marcel·lí Domingo s/n, N5, 43007 Tarragona, Spain

[‡]Medcom Advance SA, Viladecans Busines Park, Edificio Brasil, C/Bertran i Musitu, 83-85, 08840 Viladecans, Barcelona, Spain

[§]Laboratorio de Microscopias Avanzadas (LMA), Instituto de Nanociencia de Aragon (INA), Universidad de Zaragoza, 50018 Zaragoza, Spain

[∥]Fundación ARAID, 50018 Zaragoza, Spain

[⊥]Department of Biomedical Experimental and Clinical Sciences, University of Florence, 50134 Florence, Italy

[#]Institute of Applied Physics Nello Carrara, National Research Council, via Madonna del Piano 10, 50019 Sesto Fiorentino, Italy

[○]ICREA, Passeig Lluís Companys 23, 08010 Barcelona, Spain

Supporting Information

ABSTRACT: Protein misfolded proteins are among the most toxic endogenous species of macromolecules. These chemical entities are responsible for neurodegenerative disorders such as Alzheimer's, Parkinson's, Creutzfeldt−Jakob's and different non-neurophatic amyloidosis. Notably, these oligomers show a combination of marked heterogeneity and low abundance in body fluids, which have prevented a reliable detection by immunological methods so far. Herein we exploit the selectivity of proteins to react with metallic ions and the sensitivity of surface-enhanced Raman spectroscopy (SERS) toward small electronic changes in coordination compounds to design and engineer a reliable optical sensor for protein misfolded oligomers. Our strategy relies on the functionalization of Au nanoparticle-decorated polystyrene beads with an effective metallorganic Raman chemoreceptor, composed by Al^{3+} ions coordinated to 4-mercaptobenzoic acid (MBA) with high Raman cross-section, that selectively binds aberrant protein oligomers. The mechanical deformations of the MBA phenyl ring upon complexation with the oligomeric species are registered in its SERS spectrum and can be quantitatively correlated with the concentration of the target biomolecule. The SERS platform used here appears promising for future implementation of diagnostic tools of aberrant species associated with protein deposition diseases, including those with a strong social and economic impact, such as Alzheimer's and Parkinson's diseases.

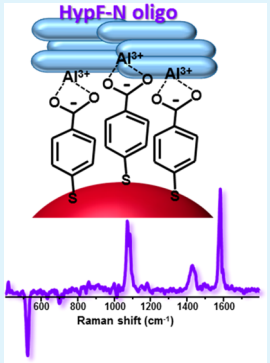

KEYWORDS: *plasmon resonance, SERS, gold, amyloid, sensor, proteins*

INTRODUCTION

The accumulation of specific peptides or proteins as misfolded amyloid fibrils is at the basis of a large number of human pathologies, ranging from neurodegenerative disorders, such as Alzheimer's and Parkinson's diseases, to non-neuropathic amyloidoses, including dialysis-related and type II diabetes amyloidoses.[1] There is increasing evidence that, at least in some protein-deposition diseases, the pathogenic species are the oligomeric assemblies that precede the formation of mature amyloid fibrils.[2,3] For example, it is now widely accepted that soluble oligomeric forms of β-amyloid, which are generated during the first stages of Alzheimer's disease, are responsible for impairing the cognitive function.[4,5] Importantly, the molecular events leading to β-amyloid oligomers are supposed to appear 10 to 20 years before the symptoms become apparent.[6,7] As a consequence, tests focused on monitoring aberrant protein oligomers are expected to represent a promising tool for diagnosing protein misfolding diseases in their earliest, presymptomatic, and most treatable stages.

The interest in detecting aberrant oligomers present in body fluids has grown strongly in recent years. Most of the detection methods proposed recently are based on enzyme-linked immunosorbent assays (ELISA) that rely on using labeled antibodies to capture and quantify the protein. These methods have been popular during the last years;[8,9] however, the risks of detecting false positives and of inaccurate determinations of the toxic species have been reported by some authors.[10,11] Additionally, the preparation of reliable substrates for oligomer detection involves several critical steps,[12] which, de facto, has

Received: October 17, 2014
Accepted: April 21, 2015
Published: April 21, 2015

DOI: 10.1021/acsami.5b01056
ACS Appl. Mater. Interfaces 2015, 7, 9420−9428

prevented ELISA assays from moving from lab to clinical practice so far.

Surface-enhanced Raman scattering (SERS) spectroscopy has emerged as a powerful ultrasensitive analytical technique in biosensing.[13−17] The SERS effect relies on huge electromagnetic fields concentrated at the nanostructured metal surface to dramatically enhance the Raman signal of molecules when localized surface plasmon resonances (LSPRs) are excited by an external incident electromagnetic wave.[18,19] Large and efficient SERS enhancements are commonly confined within ca. 2 nm from the metal surface, therefore hampering the direct acquisition of the vibrational spectra of large biomolecules, especially of those with low Raman cross sections, such as most of the proteins.[13] Additionally, the SERS spectroscopy of proteins usually yields extremely complicated spectral patterns as a consequence of their inherent molecular complexity and the varied composition of their surrounding media. This often poses severe obstacles in sample-to-sample reproducibility. To overcome such limitations, several indirect SERS-based methods have been developed.[13−16,20] As opposed to direct SERS,[21] these strategies do not acquire the characteristic vibrational fingerprint of the biomolecule but usually exploit molecular receptors anchored to the plasmonic surface to selectively bind the target molecule. This recognition event is then followed by a change in the Raman spectrum of a SERS-active molecule (also indicated as Raman probe or reporter) that indirectly inform about the presence of the biomolecule and, possibly, its concentration in the media. These perturbations of the SERS signal can be broadly associated either with (i) a variation of the overall intensity or (ii) an alteration of the spectral profile. In the first class of indirect biosensing approaches, the most notable example is represented by the development of SERS tags[13−16,22] combining, at least, three constitutive units: plasmonic nanoparticles as the optical enhancers; reporter molecules with high SERS cross sections; and a bioselective element (such as antibodies, DNA strands, etc.) toward the target biomolecule. SERS tags were widely used in a large set of different fashion for the detection of DNA,[23−25] proteins,[25−28] and small biomolecules.[29] In the second class of indirect SERS-based strategies, the bioselective capture agent also acts as a Raman reporter. In this case, rather than the increase or decrease of the overall SERS intensity, the structural changes induced on the chemical receptor upon complexation with the biomolecule are registered in its SERS profile and can be quantitatively correlated with the concentration of the target biomolecule. For example, vibrational changes in the SERS spectra of bacterial membrane protein receptor ZipA were used to monitor its interaction with the soluble FtsZ polymeric protein.[30] Similarly, SERS label-free detection of viral nucleoprotein was achieved by monitoring the spectral changes of a polyvalent anti-influenza aptamer immobilized onto silver nanorod arrays.[31] However, for the same reasons that can hamper the direct detection of high molecular weight biomolecules, the use of bioreceptors as dual SERS reporter/recognition elements is often limited mostly due to size and low cross-section. Very recently, a few works[32−34] have reported a novel attractive strategy based on the use of bioreceptors, such as an antibody or a protein, chemically modified to incorporate into the lower extremity a highly SERS-active aromatic linker that firmly binds the plasmonic surface. As a result, the SERS spectrum of the functionalized receptor is dominated by the features of the linker, which, upon the binding event with the target biomolecule, undergo distinctive changes associated with the mechanical deformation of the aromatic ring.[32−34] In this case, the Raman reporter acts as an effective molecular spring sensitive to the structural rearrangements imposed by the formation of the receptor/analyte complex.

In this article, we demonstrate the potential use of SERS for the detection of toxic aberrant protein oligomeric species exploiting the selective high affinity of these species toward specific transition metallic ions. The proposed SERS platform rests on the sensing properties of hybrid gold-decorated polystyrene beads (PS@Au) that are engineered with an effective metallorganic Raman chemoreceptor, composed by Al^{3+} ions coordinated to 4-mercaptobenzoic acid (MBA). The thiol group of MBA firmly binds the gold surface via Au−S covalent bonds, whereas the carboxylic groups of MBA chelate the Al^{3+} ions forming a coordination complex and offering effective adsorption sites for oligomer interaction. Al^{3+} ions are known to exert a marked complexation activity against proteins such β-amyloid[35,36] and promote a sort of "freezing" of the peptide structure in its oligomeric state[37] by increasing its surface hydrophobicity.[38] The SERS platform was tested on oligomers formed from the N-terminal domain of the *Escherichia coli* protein HypF (HypF-N). This 91-residue small protein is a valuable model system as it was shown to form amyloid-like fibrils similar to those associated with diseases as well as toxic oligomers.[39,40] In addition, a particular type of HypF-N oligomer called type A oligomers, were found to cause cell dysfunction, colocalize with synapses in rat hippocampus primary neurons, inhibit long-term potentiation in rat hippocampal slices, and cause cognitive impairment when injected in rats' brains, thus reproducing all the biological effects of Aβ oligomers.[41−43] Importantly, type A oligomers are sufficiently stable to maintain their structure and properties in different experimental conditions.[44] The latter feature is beneficial for a profitable setting up of a reliable and solid experimental methodology. The structural deformation imposed by the adsorption of the oligomeric proteins on the metallorganic MBA-Al^{3+} complex leads to characteristic changes in its SERS profile, which can be quantitatively correlated with the concentration of the HypF-N oligomers.

EXPERIMENTAL SECTION

Materials. HypF-N was expressed and purified as described previously.[43] Apo-Transferrin human, Holo-Transferrin human, IgG from human serum, and α-Crystallin from bovine eye lens were purchased from Sigma-Aldrich. All the other chemicals were purchased from Sigma-Aldrich and used as received. Milli-Q water was used throughout the experiments.

Synthesis of PS@Au Microbeads. The fabrication of the PS@Au microbeads was performed as previously described.[45] First, gold nanoparticles of ca. 55 nm diameter were synthesized by a seeded growth method.[46] As a first step, 15 nm diameter gold nanoparticle seeds were prepared via the common Turkevich−Frens method.[47,48] An aqueous solution of trisodium citrate (1% w/w, 4.5 mL) was added under vigorous stirring to a boiling solution of $HAuCl_4$ trihydrate (15 mg in 150 mL of milli-Q water). After 30 min under reflux, the mixture was allowed to cool to room temperature. Growth process of the gold seeds was performed by quickly adding 3.75 mL of the 15 nm gold nanoparticles and 2.56 mL of an aqueous solution of trisodium citrate (1% w/w) to 125 mL of a boiling solution of $HAuCl_4$ trihydrate (14.57 mg) in milli-Q water. The mixture was refluxed for 30 min before the addition of an extra-aliquot of trisodium citrate solution (8.6 mL, 2.3% w/w). The solution was left boiling for another hour and then let to cool to room temperature.

DOI: 10.1021/acsami.5b01056
ACS Appl. Mater. Interfaces 2015, 7, 9420−9428

Three micrometer diameter polystyrene microbeads (PS) were wrapped with alternating polyelectrolyte monolayers via a layer-by-layer electrostatic self-assembly protocol.[30,49] 0.5 mL of a 100 mg/mL PS suspension was added to 25 mL of a 2 mg/mL polystyrenesulfonate (PSS, Mw = 1 000 000) solution containing 0.5 M NaCl. The mixture was sonicated for 30 min and left under mild shaking for another 2 h. Then, three centrifugation/washing cycles were performed to remove the excess of unbound polymer from the PS beads. Identical protocol was applied for depositing subsequent layers of branched-polyethylenimine (PEI, Mw = 25 000) polyelectrolytes, and then again in an alternate fashion PSS and PEI polymers. The polyelectrolytes-wrapped PS beads were finally redispersed in 10 mL of Milli-Q water (final concentration 5 mg/mL).

The adsorption of 55 nm gold nanoparticles to the so-functionalized microbeads was accomplished by simply adding a large excess of colloids (25 mL) to 1 mL of PS beads 5 mg/mL under sonication. After 30 min of sonication followed by 2 h of shaking, the beads were left decanting overnight. The reddish color of the supernatant ensures the full saturation of the bead surface with gold nanoparticles. The precipitate was extensively washed three times with milli-Q water by centrifugation (2000 rpm, 25 min) followed by three steps of decantation to remove any unbound nanoparticles from the mixture. Finally, the PS@Au beads were redispersed to 1 mL in Milli-Q (5 mg/mL final concentration).

Functionalization of PS@Au Beads with 4-Mercaptobenzoic Acid and Al^{3+}. Functionalization of PS@Au beads with MBA was achieved by addition of 1 mL of PS@Au beads (5 mg/mL) to 9 mL of a 1×10^{-2} M ethanolic solution of MBA. The mixture was placed for 24 h on a wheel for agitation and repeatedly sonicated during this time to guarantee the optimal dispersion of the beads. Removal of the unbound MBA from solution was ensured by three centrifugation/washing cycles with ethanol followed by three centrifugation/washing cycles with milli-Q. At the end of this washing step, PS@Au@MBA beads were redispersed in 2 mL of milli-Q water (2.5 mg/mL). 0.5 mL of such suspension were then added to 5 mL of a 5 mM aqueous solution of $AlCl_3$ to promote the coordination of Al^{3+} on MBA molecules (PS@Au@MBA-Al^{3+}). The mixture was sonicated for 20 min and then left under agitation for 3 h before being exposed to three centrifugation/washing cycles with 10 mL of milli-Q water. PS@Au@MBA-Al^{3+} beads were finally redispersed in 10 mL of milli-Q water (0.25 mg/mL).

Functionalization of Au Nanoparticles with 4-Mercaptobenzoic Acid and Al^{3+} for SR-EELS Measurements. A solution containing 176 μL of NaOH (29% aqueous solution) and 15 μL of MBA (5 mM in EtOH) was rapidly added under vigorous stirring to 10 mL of gold colloids ([Au^0] = 0.3 mM). The MBA concentration (ca. 15 molecules per nm^2) was calculated to provide a full coating of the gold surface (ca. 2.3 molecules per nm^2). The solution was left under gentle stirring for another 30 min to allow full MBA adsorption onto the gold surface (Au@MBA). Subsequently, 15 μL of a $AlCl_3$ 5 mM aqueous solution was added under stirring to the colloidal suspension and then left aging overnight to yield the corresponding Au@MBA-Al^{3+} nanoparticles. One centrifugation cycle (5.4 K, 30 min) was performed to remove the excess of unbound MBA and Al^{3+} ions. The resulting nanoparticles were redispersed in 10 mL of Milli-Q water. Supporting Information, Figure S1 illustrates the extinction spectra of the gold colloids at different stages of the surface functionalization, showing that a minimal broadening of the LSPR occurs during the process (i.e., the nanoparticles preserve their colloidal stability with marginal formation of aggregates). Finally, 10 μL of phosphate buffered solution (24 mM, pH 7) of HypF-N oligomers were added to 50 μL of Au@MBA-Al^{3+} colloidal suspension. Samples were left unperturbed overnight before being investigated by spatially resolved electron energy loss spectroscopy (SR-EELS).

Transmission Electron Microscopy. The transmission electron microscopy (TEM) samples were prepared by dispersing the nanoparticle powders in ethanol. The dispersions were ultrasonicated and subsequently deposited on holey carbon 3 mm copper grids.

Surface-Enhanced Raman Spectroscopy Detection of Proteins. Phosphate-buffered solution (10 μL, 24 mM, pH 7) of HypF-N oligomers, Apo-Transferrin, Holo-Transferrin, IgG, and α-crystallin at different concentrations, were added to 50 μL of sonicated PS@Au@MBA-Al^{3+} suspension. Samples were left unperturbed overnight and then investigated by SERS using a 785 nm laser and a long working distance objective (ca. 30 mW laser power, 5 accumulations, 10 s exposure time). HypF-N type A toxic oligomers are prepared as previously reported.[43] Because of the difficulty of producing highly concentrated solutions of stable HypF-N oligomers, the SERS analysis was limited to the 0 to 1.2 μM range (final concentration of the corresponding monomer in the investigated sample).

Instrumentation. SERS experiments were conducted using a Renishaw InVia Reflex confocal microscope equipped with a high-resolution grating with 1200 grooves/cm for near-IR wavelengths, additional band-pass filter optics, and a CCD camera. UV−vis spectra were recorded using a Thermo Scientific Evolution 201 UV−visible spectrophotometer. Environmental scanning electron microscopy (ESEM) was performed with a JEOL 6400 scanning electron microscope.

SR-EELS measurements were performed on probe-corrected scanning TEM (STEM) FEI Titan Low-Base 60−300 operating at 80 keV (fitted with a X-FEG gun and Cs-probe corrector (CESCOR from CEOS GmbH)). Furthermore, to avoid the effects of electron beam damage, these measurements were performed using a liquid-nitrogen-cooled cryo-holder at −170 °C. EEL spectra were recorded using the spectrum-imaging (SPIM in 2D or spectrum-line (SPLI) in 1D) mode[50,51] in a Gatan GIF Tridiem ESR 865 spectrometer. The convergent semiangle was of 25 mrad, the collection semiangle was of 20 mrad, and the energy resolution was ∼1.2 eV.

RESULTS AND DISCUSSION

A robust and highly SERS-active composite material consisting of PS beads of 3 μm in diameter fully loaded with gold nanoparticles of ∼55 nm (Au) in diameter was synthesized as described elsewhere.[45] The external dense shell of interacting nanoparticles concentrates a large number of hot-spots on each bead. As a result, the averaged SERS enhancement performance has been shown to have very good bead-to-bead homogeneity.[52,53] Furthermore, all the SERS measurements reported in this study were obtained under an averaged bulk SERS regime.[54] In our experimental setup, the laser simultaneously investigates a large ensemble of beads in suspension within the scattering volume of a long working distance objective. The averaging effect of these numerous contributions is a critical factor for obtaining ensemble signals that are stable and reproducible. Figure 1A,B shows representative ESEM and TEM images, respectively, of a single PS@Au bead. Figure 1C illustrates the shift of the plasmon resonance of the isolated Au nanoparticles from 536 to 550 nm upon assembly onto the bead surfaces (PS@Au) as a result of the plasmonic coupling of adjacent nanoparticles.

The gold surfaces in the PS@Au substrates were further functionalized by immersion into a 5 mM ethanolic solution of MBA. MBA molecules self-assemble into a dense monolayer over the metal surface adopting a preferable perpendicular orientation with respect to the gold surface and exposing the carboxylate groups toward the bulk solution[55] (Figure 2). The resulting functionalized PS@Au particles are called here PS@Au@MBA. In our sensing scheme, the aim of the chemical modification of the PS@Au particles with MBA is twofold: to introduce carboxylate groups as chelating moieties for Al^{3+} immobilization and provide the sensing platform with an effective Raman probe whose intense SERS spectrum is sensitive to changes in metal ion coordination.[56] Metal ion coordination with the COO^- moiety of MBA leads to characteristic spectral changes, as illustrated in Figure 2A

DOI: 10.1021/acsami.5b01056
ACS Appl. Mater. Interfaces 2015, 7, 9420−9428

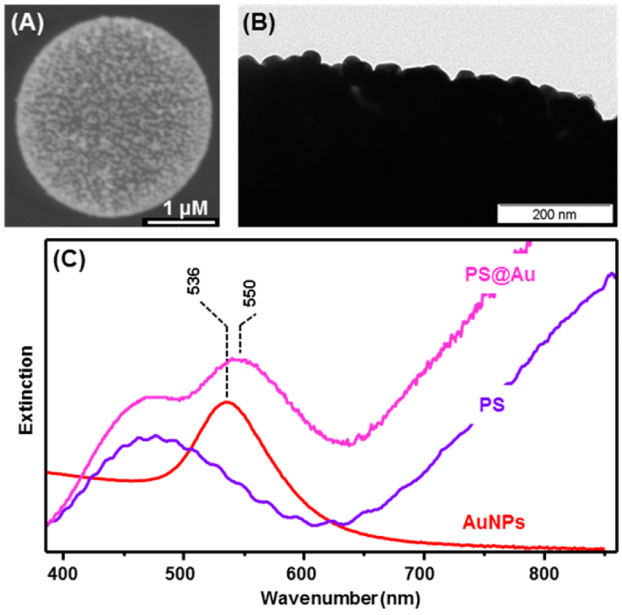

Figure 1. Representative (A) SEM and (B) TEM images of PS@Au beads. (C) Extinction spectra of the AuNPs, PS, and PS@Au suspensions (the intensity of the spectra was modified for comparison).

where the normalized SERS spectra of PS@Au@MBA before and after the exposure to a 5 mM $AlCl_3$ water solution are compared. The SERS spectrum of MBA is dominated by the ring modes at 1589, 1079, and 522 cm^{-1}, explicitly assigned to C═C stretching, ring breathing, and out-of-plane ring deformation, respectively.[55,57] However, the main spectral changes resulting from the metal ion coordination are observed in those Raman bands associated with the carboxylic group. Specifically, we observe a marked decrease of the C═O stretching contribution at 1702 cm^{-1}, a drastic shift of the symmetric stretching of the COO^- moiety from 1395 to 1436 cm^{-1}, and a similar shift of the band at 844 cm^{-1}, ascribed to the COO^- scissoring mode, up to 857 cm^{-1}. In particular, the COO^- symmetric stretching was shown to be extremely sensitive to changes in local pH[58] as well as metal ion coordination.[56] Differently from what observed for other organic molecules,[59] the coordination of Al^{3+} on MBA does not cause the appearance of any new vibrational features in the ligand SERS spectrum. Therefore, the corresponding ratio of the peak intensities at 1436 and 1395 cm^{-1} (I_{1436}/I_{1395}) represents a truly spectral marker for the monitoring of the MBA-Al^{3+} complex formation. The inset in Figure 2B describes the evolution of the I_{1436}/I_{1395} spectral ratio as a function of Al^{3+} concentration: detection of Al^{3+} can be achieved below the nanomolar regime, whereas saturation was observed above 1×10^{-4} M for PS@Au@MBA concentrations of 0.25 mg/mL.

In the previous report,[56] MBA was used as an effective SERS-active chemoreceptor for the identifications of metal ions in +1 and +2 oxidation state. Thus, as an intermediate result of the construction of the metallorganic-decorated plamonic hybrid composite for toxic protein oligomers detection, we also report the first example of SERS identification and quantification of Al^{3+} by using MBA as effective chemoreceptor. Importantly, metal ion chelation to MBA is known to induce, especially in its carboxylate-associated vibrations, spectroscopic shifts that are specific to the coordinated analyte[56,60] (Figure 2C and Supporting Information, Figure S2). The recognition of these

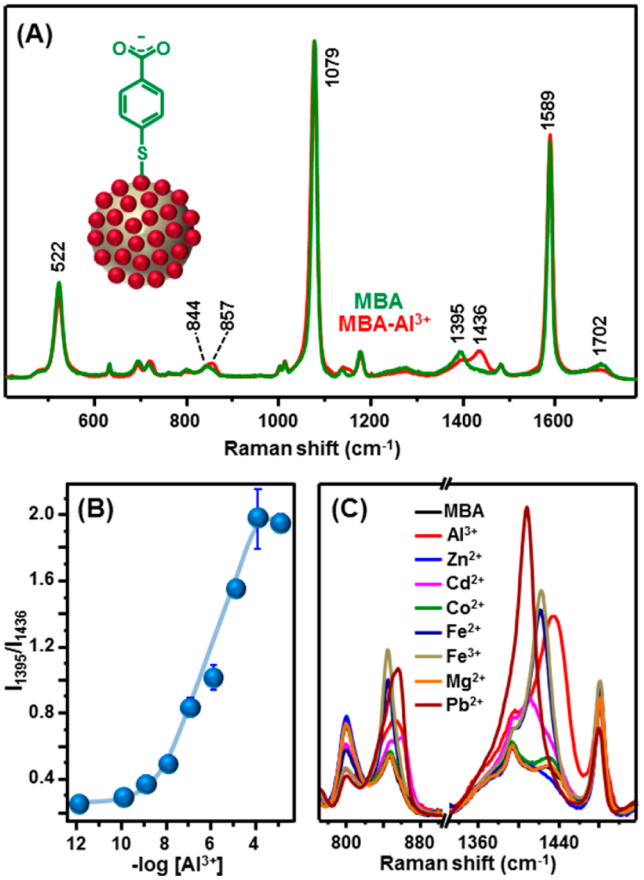

Figure 2. (A) Normalized SERS spectra of 0.25 mg/mL PS@Au@MBA beads before and after the exposure to 5 mM $AlCl_3$. An outline of the sensing platform is also included (at neutral pH, the carboxylic group exists in the deprotonated form, $pK_a = 4.19$). (B) Ratio between the intensities of the bands at 1395 and 1436 cm^{-1} is plotted against the Al^{3+} concentration (logarithmic scale). Error bars equal to two standard deviations ($N = 3$). (C) Details of the 770−890 cm^{-1} and 1330−1520 cm^{-1} spectral ranges for SERS spectra of 0.25 mg/mL PS@Au@MBA beads before and after the exposure to 1 mM aqueous solutions of: $AlCl_3$, $ZnCl_2$, $FeCl_2$, $FeCl_3$, $CoCl_2$, $Cu(NO_3)_2$, $CdCl_2$, $MgSO_4$, and $PbCl_2$.

different spectroscopic patterns is at the basis of the multiplex SERS detection of different metal ions with MBA-functionalized plasmonic surfaces.[56]

The SERS platform was then tested by exposing the fully aluminum saturated PS@Au@MBA-Al^{3+} beads to phosphate-buffered solutions of misfolded HypF-N type A toxic oligomers (final protein concentration 1.2 μM). The SERS spectrum of PS@Au@MBA-Al^{3+} in phosphate buffer (blank) shows rather subtle differences with respect to those acquired in the presence of HypF-N oligomers (Figure 3), which can be however fully disclosed by digital removal of the blank signal. The resulting difference spectrum (Δ Oligo HypF-N) highlights several spectral changes in the MBA (Figure 3). In addition to a relative intensity increase in the metal ion-coordinated COO^- symmetric stretching at 1436 cm^{-1}, the difference SERS profile reveals, among others, a relative intensity increase and slight shift to lower wavenumbers of the C═C stretching at 1589 cm^{-1}, an opposing drop in the 522 cm^{-1} band intensity, whereas the ring breathing band at 1079 cm^{-1} undergoes an increase in bandwidth. These changes are consistent with the binding of the large oligomeric species to the metallorganic

DOI: 10.1021/acsami.5b01056
ACS Appl. Mater. Interfaces 2015, 7, 9420−9428

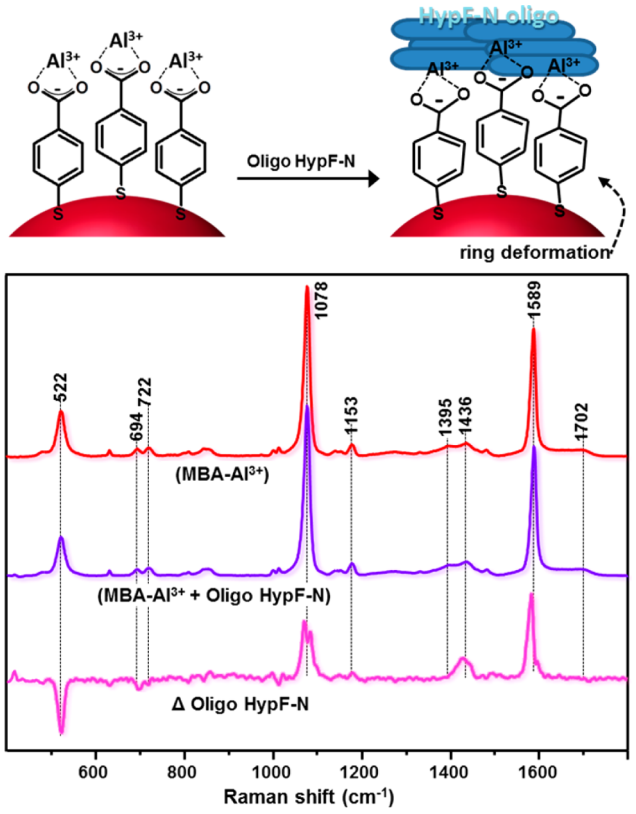

Figure 3. Normalized SERS spectra of the PS@Au@MBA-Al^{3+} suspension before (red curve) and after (violet curve) the addition the HypF-N oligomer in phosphate buffer (final protein concentration of 1.5 μM). The corresponding difference spectrum (ΔOligo HypF-N, pink curve) was obtained by digital subtraction of the (MBA-Al^{3+}) spectrum from the (MBA-Al^{3+} + Oligo HypF-N) spectrum. Prior to the subtraction, all the spectra were normalized to the ring breathing band at 1079 cm^{-1}. Top scheme: outlines of the oligo HypF-N coordination onto PS@Au@MBA-Al^{3+} beads.

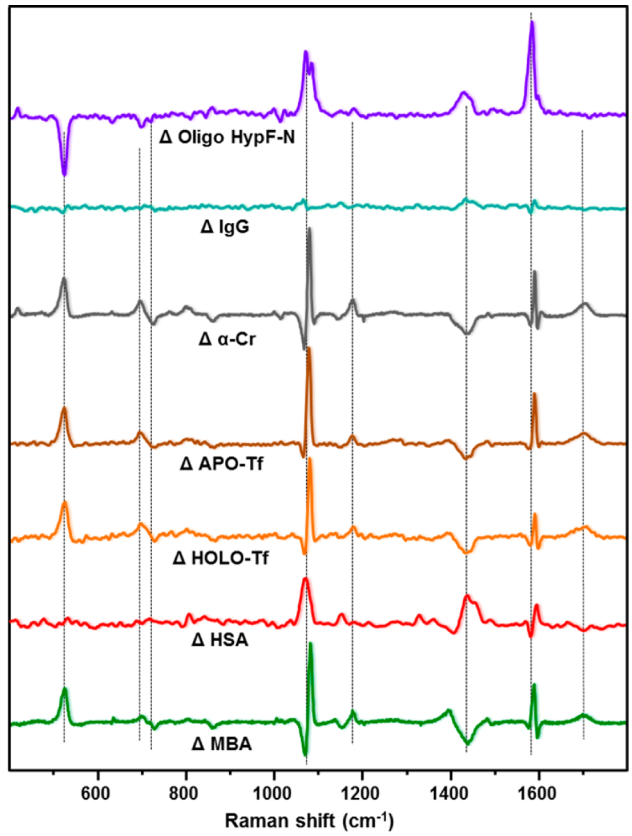

Figure 4. Digitally subtracted spectra obtained by subtracting the MBA-Al^{3+} spectrum shown in Figure 3, from the SERS spectra of: HypF-N oligomer, immunoglobulin G (IgG); α-crystallin (α-Cr); APO- and HOLO-transferrin (APO-Tf and HOLO-Tf); and human serum albumin (HSA). The final protein concentration was 1.5 μM for HypF-N oligomer and 2.5 μM for the remaining proteins. The spectrum ΔMBA is the result of the digital subtraction of MBA-Al^{3+} from the spectrum of MBA in the absence of Al^{3+}. Prior to the subtraction, all the spectra were normalized to the ring breathing band at 1079 cm^{-1}.

chemoreceptor leading to a mechanical deformation of the MBA phenyl ring sandwiched between the adsorbed biomolecule and the metal surface (Figure 3).[32−34] As a control experimentl, PS@Au@MBA beads were exposed to HypF-N oligomers. Their corresponding SERS spectra (Supporting Information, Figure S3) do not reveal significant alterations upon the addition of the toxic oligomers, indicating that no significant interaction takes place in the absence of Al^{3+}.

The possibility of a selective detection of aberrant oligomers by our sensor was investigated over different proteins, including immunoglobulin G (IgG) and transferrin (HOLO-Tf and APO-Tf), which are typically found in serum and cerebrospinal fluid,[61] human serum albumin (HSA), and of a small heat shock protein, α-crystallin (α-Cr), which is known to colocalize with aberrant oligomer deposits[62,63] and to have solvent-exposed hydrophobic moieties similarly to aberrant protein oligomers.[64]

The difference spectra for the other proteins are shown in Figure 4 and reveal rather different spectral changes with respect to those observed for the toxic oligomers. Apart from the case of IgG, which appears to leave unperturbed the surface complex MBA-Al^{3+}, we observe a very similar, unspecific spectral pattern for α-Cr and HOLO- and APO-Tf. Interestingly, the set of changes of the SERS profile perfectly matches those observed upon removal of Al^{3+} from the beads (see the ΔMBA difference spectrum in Figure 4, which is the result of the digital subtraction of the SERS spectrum of MBA-Al^{3+} from the SERS spectra of the free MBA ligand). These data suggest a partial removal of the coordinated Al^{3+} ions from the carboxylic groups upon addition of α-Cr and transferrin proteins, which could be the result of different processes, such as the sequestration of metal ions from unbound proteins in the bulk solution, followed or not by their subsequent adhesion onto the metal surface. Finally, the set of features in the HSA difference spectrum further diverge from the rest illustrated in Figure 4, revealing a spectral pattern that appears to be somehow intermediate between the toxic oligomers and the other proteins. It has been shown that bovine serum albumin can perturb the SERS spectra of MBA adsorbed on silver surfaces even though the exact mechanism has not yet been elucidated.[65] In any case, the intense vibrational fingerprint of the metallorganic Raman chemoreceptor undergoes characteristic spectral changes upon selective anchoring of HypF-N aberrant oligomers, while other protein species induce null or different, nonspecific perturbations.

The efficiency of the retention of the HypF-N oligomers and their distribution was also studied with SR-EELS measurements.[66−68] Because of the physical impossibility of operating the experiments directly on microbeads, the SR-EELS analysis was performed using, as a sensing substrate, monodispersed

DOI: 10.1021/acsami.5b01056
ACS Appl. Mater. Interfaces 2015, 7, 9420−9428

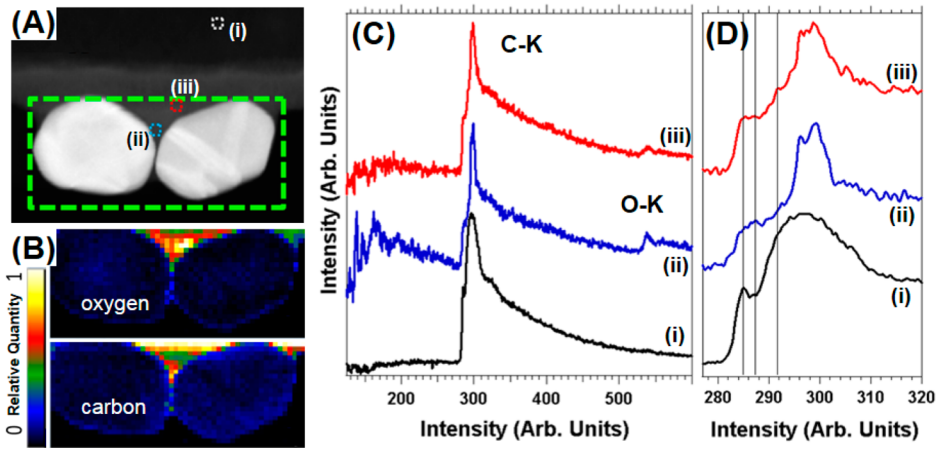

Figure 5. (A) HAADF image of a couple of Au particles exposed to the oligomer solution. EELS-SPIM was recorded in the marked green area of this micrograph. (B) Carbon and oxygen elemental maps extracted from the SPIM after background subtraction. (C) EEL spectra collected in the HAADF-image in the marked areas denoted as (i), (ii), and (iii). (i) is a reference recorded in the carbon membrane. The C−K edge is visible in all the spectra. The O−K edge is only visible in the spectra (ii) and (iii). (D) C−K edge fine structures (ELNES) extracted from the EEL spectra of (C).

gold nanoparticles functionalized with a monolayer of the metallorganic complex MBA-Al^{3+} in place of hybrid PS@Au@MBA-Al^{3+} microparticles. The experiments were performed under cryogenic conditions (−170 °C) and low acceleration voltage (80 kV).[68] An EELS spectrum-image (SPIM) was acquired in the green marked area depicted in the high angle annular dark field (HAADF)-STEM image (Figure 5A). Chemical maps of carbon and oxygen were extracted from the EELS-SPIM (Figure 5B). The analysis of the elemental maps reveals clear correlations between C and O, which are localized at specific areas on the surface of the functionalized NP. Figure 5C displays three EEL spectra extracted in the white, blue, and red areas marked in Figure 5A, respectively. Carbon K edge is present in all of these three EEL spectra. By comparing the energy loss near-edge fine structures (ELNES) of the C−K edge from three areas of the sample: (i) corresponds to the supporting carbon film of the TEM grid, while (ii) and (iii) correspond to areas where the organic materials are localized (Figure 5B). The C−K ELNES signal of the supporting C membrane was used as reference. This signal corresponds to amorphous carbon showing the characteristic as fingerprints of sp^2 carbons at 285 eV (π^*) and a band starting at 292 eV (σ^*).[67] ELNES features acquired in the areas (ii) and (iii) differ significantly from those of amorphous carbon. Besides the peak at 285 eV, two other signatures can be observed in Figures 5D (ii) and (iii) at 288 and 291.5 eV. The 288 eV contribution can be assigned to C═C π^* (from CH_2 groups, after reduction by the electron beam) or to C═O π^* excitations.[68] The signal at 291.5 eV correspond to C═O π^* excitations.[68] In addition, the features corresponding to the σ^* excitations (band formed by two peaks at ∼295 and ∼299 eV) are very different to these ones of the graphitic or amorphous sp^2 carbons.[66] Since analysis over 1000 eV is not feasible due to the low signal-to-noise ratio, Al cannot be assessed at the present concentrations. The signals of C and O nanometers far from the surface (Figure 5B) indicate the positive retention of HypF-N oligomers on the NPs surface.

To assess the existence of a quantitative correlation between the concentration of HypF-N oligomers and the spectral changes illustrated in Figure 6, the intensity difference between the positive C═C stretching mode at 1589 cm^{-1} and the

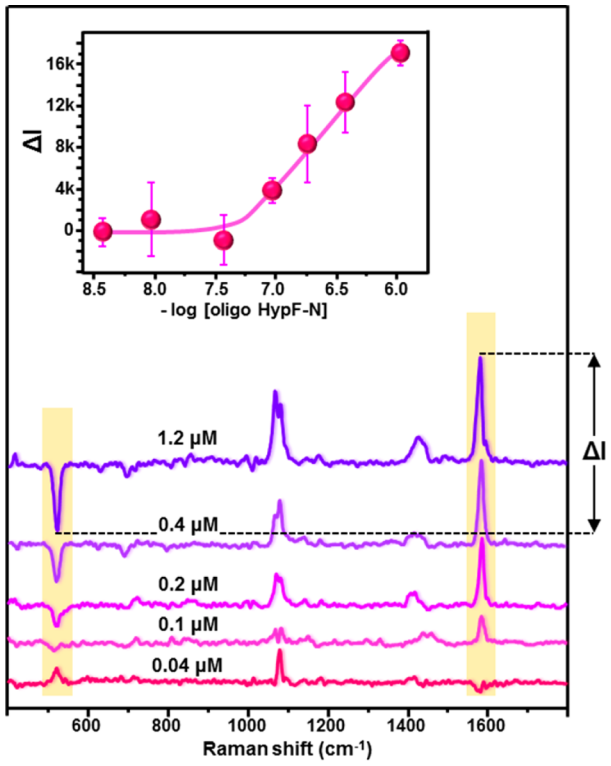

Figure 6. Difference SERS spectra, ΔOligo HypF-N, obtained for different HypF-N concentrations. The difference spectra were obtained by digital subtraction of the (MBA-Al^{3+}) spectrum from the (MBA-Al^{3+} + Oligo HypF-N) spectra acquired at a final protein concentration of: 1.2, 0.4, 0.2, 0.1, and 0.04 μM. Prior to the subtraction, all the spectra were normalized to the ring breathing band at 1079 cm^{-1}. (inset) Dependence of the intensity difference between the bands at 1589 and 522 cm^{-1} (ΔI) on HypF-N oligomer concentration. Error bars equal to two standard deviations (N = 3).

negative out-of-plane ring deformation at 522 cm^{-1} (ΔI) was selected as a spectral marker. The plot of the ΔI values versus oligomer concentration (Figure 6, inset) shows a linear correlation (r^2 > 0.98) and detection limit of 0.1 μM, which corresponds to less than 6 pmol in the analyzed sample volume

DOI: 10.1021/acsami.5b01056
ACS Appl. Mater. Interfaces 2015, 7, 9420−9428

(60 μL). It is worth of noting, however, that the actual volume investigated by the laser focused onto the sample is below the sub-microliter range under the current experimental conditions,[17,69] and, therefore, the corresponding amount of analyzed oligomers is in the subpicomole regime.

CONCLUSION

The proposed method is rapid, reliable, and easy to set up and perform, circumventing a number of problems typically associated with previous analytical methods, such as ELISA assays. In fact, ELISAs based on amyloid capture by using specific antibodies have been mainly proposed for the detection of amyloid oligomers during the past decade. However, positive initial results were rarely supported by follow-up studies, which might be due to technical difficulties of the protocols that contain several critical steps in sample preparation with antibodies and measurement procedures. An additional disadvantage of ELISA assays is the presence of heterophilic antibodies in body fluids, which recognize immunoglobulins of other species. As a result, false-positive results or underestimation of the amyloid species are generated.

The present work has been performed on HypF-N type A toxic oligomers, which have the advantage of reproducing all biological effects of Aβ oligomers but, unlike these, are very stable and are thus amenable to experimental investigation. The MBA-Al^{3+} chemoreceptor decorating PS@Au beads undergoes mechanical deformations of its phenyl ring upon complexation with HypF-N oligomer species, which are registered in their SERS spectrum and serve for their quali-quantitative detection. This is not the case of other body fluid compounds here tested and that include antibodies, metal-binding proteins, and species colocalized with toxic protein oligomers in the body.

In summary, the SERS platform used here appears promising for future implementation of diagnostic tools of aberrant oligomer species associated with protein-deposition diseases, including those with a strong social and economic impact, such as Alzheimer's and Parkinson's diseases.

ASSOCIATED CONTENT

Supporting Information

Extinction spectra of Au colloids at different stages of the surface functionalization; SERS spectra of PS@Au@MBA in the presence of different metal ions; SERS spectra of the PS@Au@MBA upon addition of HypF-N oligomer; discussion of direct versus indirect SERS detection of fibril proteins. The Supporting Information is available free of charge on the ACS Publications website at DOI: 10.1021/acsami.5b01056.

AUTHOR INFORMATION

Corresponding Authors

*E-mail: ramon.alvarez@urv.cat. (R.A.A.-P.)
*E-mail: p.matteini@ifac.cnr.it. (P.M.)

Notes

The authors declare no competing financial interest.

ACKNOWLEDGMENTS

This work was funded by the Spanish Ministerio de Economia y Competitividad (CTQ2011-23167 and FIS2013-46159-C3-3-P), the European Research Council (CrossSERS, FP7/2013 329131, PrioSERS FP7/2014 623527, and ESTEEM2-312483), and Medcom Advance SA. The transmission electron microscopy work was conducted in the Laboratorio de Microscopias Avanzadas at the Instituto de Nanociencia de Aragon, Universidad de Zaragoza (Spain).

REFERENCES

(1) Chiti, F.; Dobson, C. M. Protein Misfolding, Functional Amyloid, and Human Disease. *Annu. Rev. Biochem.* **2006**, *75*, 333−366.
(2) Kayed, R.; Head, E.; Thompson, J. L.; McIntire, T. M.; Milton, S. C.; Cotman, C. W.; Glabe, C. G. Common Structure of Soluble Amyloid Oligomers Implies Common Mechanism of Pathogenesis. *Science* **2003**, *300*, 486−489.
(3) Sousa, M. M.; Saraiva, M. J. Neurodegeneration in Familial Amyloid Polyneuropathy: From Pathology to Molecular Signaling. *Prog. Neurobiol.* **2003**, *71*, 385−400.
(4) Trends in Biochemical Sciences Cleary, J. P.; Walsh, D. M.; Hofmeister, J. J.; Shankar, G. M.; Kuskowski, M. A.; Selkoe, D. J.; Ashe, K. H. Natural Oligomers of the Amyloid-β Protein Specifically Disrupt Cognitive Function. *Nature Neurosci.* **2005**, *8*, 79−84.
(5) Larson, M. E.; Lesné, S. E. Soluble Aβ Oligomer Production and Toxicity. *J. Neurochem.* **2012**, *120*, 125−139.
(6) Ganguli, M.; Rodriguez, E.; Mulsant, B.; Richards, S.; Pandav, R.; Bilt, J. V.; Dodge, H. H.; Stoehr, G. P.; Saxton, J.; Morycz, R. K.; Rubin, R. T.; Farkas, B.; DeKosky, S. T. Detection and Management of Cognitive Impairment in Primary Care: The Steel Valley Seniors Survey. *J. Am. Geriatr. Soc.* **2004**, *52*, 1668−1675.
(7) Knopman, D. S.; DeKosky, S. T.; Cummings, J. L.; Chui, H.; Corey-Bloom, J.; Relkin, N.; Small, G. W.; Miller, B.; Stevens, J. C. Practice Parameter: Diagnosis of Dementia (an Evidence-Based Review): Report of the Quality Standards Subcommittee of the American Academy of Neurology. *Neurology* **2001**, *56*, 1143−1153.
(8) Paleologou, K. E.; Kragh, C. L.; Mann, D. M. A.; Salem, S. A.; Al-Shami, R.; Allsop, D.; Hassan, A. H.; Jensen, P. H.; El-Agnaf, O. M. A. Detection of Elevated Levels of Soluble α-Synuclein Oligomers in Post-Mortem Brain Extracts from Patients with Dementia with Lewy Bodies. *Brain* **2009**, *132*, 1093−1101.
(9) Yang, T.; Hong, S.; O'Malley, T.; Sperling, R. A.; Walsh, D. M.; Selkoe, D. J. New Elisas with High Specificity for Soluble Oligomers of Amyloid β-Protein Detect Natural Aβ Oligomers in Human Brain but Not Csf. *Alzheimer's Dementia* **2013**, *9*, 99−112.
(10) Sehlin, D.; Söllvander, S.; Paulie, S.; Brundin, R.; Ingelsson, M.; Lannfelt, L.; Pettersson, F. E.; Englund, H. Interference from Heterophilic Antibodies in Amyloid-β Oligomer Elisas. *J. Alzheimer's Dis.* **2010**, *21*, 1295−1301.
(11) Stenh, C.; Englund, H.; Lord, A.; Johansson, A.-S.; Almeida, C. G.; Gellerfors, P.; Greengard, P.; Gouras, G. K.; Lannfelt, L.; Nilsson, L. N. G. Amyloid-B Oligomers Are Inefficiently Measured by Enzyme-Linked Immunosorbent Assay. *Ann. Neurol.* **2005**, *58*, 147−150.
(12) Bruggink, K. A.; Jongbloed, W.; Biemans, E. A. L. M.; Veerhuis, R.; Claassen, J. A. H. R.; Kuiperij, H. B.; Verbeek, M. M. Amyloid-B Oligomer Detection by ELISA in Cerebrospinal Fluid and Brain Tissue. *Anal. Biochem.* **2013**, *433*, 112−120.
(13) Alvarez-Puebla, R. A.; Liz-Marzan, L. M. SERS-Based Diagnosis and Biodetection. *Small* **2010**, *6*, 604−610.
(14) Xie, W.; Schlücker, S. Medical Applications of Surface-Enhanced Raman Scattering. *Phys. Chem. Chem. Phys.* **2013**, *15*, 5329−5344.
(15) Bantz, K. C.; Meyer, A. F.; Wittenberg, N. J.; Im, H.; Kurtulus, O.; Lee, S. H.; Lindquist, N. C.; Oh, S. H.; Haynes, C. L. Recent Progress in SERS Biosensing. *Phys. Chem. Chem. Phys.* **2011**, *13*, 11551−11567.
(16) Tripp, R. A.; Dluhy, R. A.; Zhao, Y. P. Novel Nanostructures for SERS Biosensing. *Nano Today* **2008**, *3*, 31−37.
(17) Guerrini, L.; Krpetić, Ž.; van Lierop, D.; Alvarez-Puebla, R. A.; Graham, D. Direct Surface-Enhanced Raman Scattering Analysis of DNA Duplexes. *Angew. Chem., Int. Ed.* **2015**, *54*, 1144−1148.
(18) Moskovits, M. Surface-Enhanced Spectroscopy. *Rev. Mod. Phys.* **1985**, *57*, 783−826.
(19) Alvarez-Puebla, R. A. Effects of the Excitation Wavelength on the SERS Spectrum. *J. Phys. Chem. Lett.* **2012**, *3*, 857−866.

DOI: 10.1021/acsami.5b01056
ACS Appl. Mater. Interfaces 2015, 7, 9420−9428

(20) Porter, M. D.; Lipert, R. J.; Siperko, L. M.; Wang, G.; Narayanana, R. SERS as a Bioassay Platform: Fundamentals, Design, and Applications. *Chem. Soc. Rev.* **2008**, *37*, 1001−1011.
(21) Buividas, R.; Dzingelevičius, N.; Kubiliūtė, R.; Stoddart, P. R.; Khanh Truong, V.; Ivanova, E. P.; Juodkazis, S. Statistically Quantified Measurement of an Alzheimer's Marker by Surface-Enhanced Raman Scattering. *J. Biophotonics* **2014**, DOI: 10.1002/jbio.201400017.
(22) Wang, Y. Q.; Yan, B.; Chen, L. X. SERS Tags: Novel Optical Nanoprobes for Bioanalysis. *Chem. Rev.* **2013**, *113*, 1391−1428.
(23) Guerrini, L.; McKenzie, F.; Wark, A. W.; Faulds, K.; Graham, D. Tuning the Interparticle Distance in Nanoparticle Assemblies in Suspension Via DNA-Triplex Formation: Correlation between Plasmonic and Surface-Enhanced Raman Scattering Responses. *Chem. Sci.* **2012**, *3*, 2262−2269.
(24) Krpetić, Ž.; Singh, I.; Su, W.; Guerrini, L.; Faulds, K.; Burley, G. A.; Graham, D. Directed Assembly of DNA-Functionalized Gold Nanoparticles Using Pyrrole−Imidazole Polyamides. *J. Am. Chem. Soc.* **2012**, *134*, 8356−8359.
(25) Zhang, H.; Harpster, M. H.; Park, H. J.; Johnson, P. A. Surface-Enhanced Raman Scattering Detection of DNA Derived from the West Nile Virus Genome Using Magnetic Capture of Raman-Active Gold Nanoparticles. *Anal. Chem.* **2011**, *83*, 254−260.
(26) Han, X. X.; Zhao, B.; Ozaki, Y. Surface-Enhanced Raman Scattering for Protein Detection. *Anal. Bioanal. Chem.* **2009**, *394*, 1719−1727.
(27) Bonham, A. J.; Braun, G.; Pavel, I.; Moskovits, M.; Reich, N. O. Detection of Sequence-Specific Protein-DNA Interactions Via Surface Enhanced Resonance Raman Scattering. *J. Am. Chem. Soc.* **2007**, *129*, 14572−14573.
(28) Wang, G.; Lipert, R. J.; Jain, M.; Kaur, S.; Chakraboty, S.; Torres, M. P.; Batra, S. K.; Brand, R. E.; Porter, M. D. Detection of the Potential Pancreatic Cancer Marker Muc4 in Serum Using Surface-Enhanced Raman Scattering. *Anal. Chem.* **2011**, *83*, 2554−2561.
(29) Vangala, K.; Yanney, M.; Hsiao, C. T.; Wu, W. W.; Shen, R. F.; Zou, S. G.; Sygula, A.; Zhang, D. M. Sensitive Carbohydrate Detection Using Surface Enhanced Raman Tagging. *Anal. Chem.* **2010**, *82*, 10164−10171.
(30) Ahijado-Guzman, R.; Gomez-Puertas, P.; Alvarez-Puebla, R. A.; Rivas, G.; Liz-Marzan, L. M. Surface-Enhanced Raman Scattering-Based Detection of the Interactions between the Essential Cell Division Ftsz Protein and Bacterial Membrane Elements. *ACS Nano* **2012**, *6*, 7514−7520.
(31) Negri, P.; Chen, G. J.; Kage, A.; Nitsche, A.; Naumann, D.; Xu, B. Q.; Dluhy, R. A. Direct Optical Detection of Viral Nucleoprotein Binding to an Anti-Influenza Aptamer. *Anal. Chem.* **2012**, *84*, 5501−5508.
(32) Kho, K. W.; Dinish, U. S.; Kumar, A.; Olivo, M. Frequency Shifts in SERS for Biosensing. *ACS Nano* **2012**, *6*, 4892−4902.
(33) Guerrini, L.; Pazos, E.; Penas, C.; Vázquez, M. E.; Mascareñas, J. L.; Alvarez-Puebla, R. A. Highly Sensitive SERS Quantification of the Oncogenic Protein C-Jun in Cellular Extracts. *J. Am. Chem. Soc.* **2013**, *135*, 10314−10317.
(34) Perumal, J.; Kong, K. V.; Dinish, U. S.; Bakker, R. M.; Olivo, M. Design and Fabrication of Random Silver Films as Substrate for SERS Based Nano-Stress Sensing of Proteins. *RSC Adv.* **2014**, *4*, 12995−13000.
(35) Zatta, P.; Drago, D.; Bolognin, S.; Sensi, S. L. Alzheimer's Disease, Metal Ions and Metal Homeostatic Therapy. *Trends Pharmacol. Sci.* **2009**, *30*, 346−355.
(36) Kawahara, M.; Kato-Negishi, M. Link between Aluminum and the Pathogenesis of Alzheimer's Disease: The Integration of the Aluminum and Amyloid Cascade Hypotheses. *Int. J. Alzheimer's Dis.* **2011**, *2011*, 276393.
(37) Drago, D.; Bettella, M.; Bolognin, S.; Cendron, L.; Scancar, J.; Milacic, R.; Ricchelli, F.; Casini, A.; Messori, L.; Tognon, G.; Zatta, P. Potential Pathogenic Role of β-Amyloid1−42−Aluminum Complex in Alzheimer's Disease. *Int. J. Biochem. Cell Biol.* **2008**, *40*, 731−746.
(38) Banks, W. A.; Niehoff, M. L.; Drago, D.; Zatta, P. Aluminum Complexing Enhances Amyloid β Protein Penetration of Blood-Brain Barrier. *Brain Res.* **2006**, *1116*, 215−221.
(39) Chiti, F.; Bucciantini, M.; Capanni, C.; Taddei, N.; Dobson, C. M.; Stefani, M. Solution Conditions Can Promote Formation of Either Amyloid Protofilaments or Mature Fibrils from the Hypf N-Terminal Domain. *Protein Sci.* **2001**, *10*, 2541−2547.
(40) Relini, A.; Torrassa, S.; Rolandi, R.; Gliozzi, A.; Rosano, C.; Canale, C.; Bolognesi, M.; Plakoutsi, G.; Bucciantini, M.; Chiti, F.; Stefani, M. Monitoring the Process of Hypf Fibrillization and Liposome Permeabilization by Protofibrils. *J. Mol. Biol.* **2004**, *338*, 943−957.
(41) Mannini, B.; Cascella, R.; Zampagni, M.; van Waarde-Verhagen, M.; Meehan, S.; Roodveldt, C.; Campioni, S.; Boninsegna, M.; Penco, A.; Relini, A.; Kampinga, H. H.; Dobson, C. M.; Wilson, M. R.; Cecchi, C.; Chiti, F. Molecular Mechanisms Used by Chaperones to Reduce the Toxicity of Aberrant Protein Oligomers. *Proc. Natl. Acad. Sci. U.S.A.* **2012**, *109*, 12479−12484.
(42) Tatini, F.; Pugliese, A. M.; Traini, C.; Niccoli, S.; Maraula, G.; Ed Dami, T.; Mannini, B.; Scartabelli, T.; Pedata, F.; Casamenti, F.; Chiti, F. Amyloid-B Oligomer Synaptotoxicity is Mimicked by Oligomers of the Model Protein Hypf-N. *Neurobiol. Aging* **2013**, *34*, 2100−2109.
(43) Campioni, S.; Mannini, B.; Zampagni, M.; Pensalfini, A.; Parrini, C.; Evangelisti, E.; Relini, A.; Stefani, M.; Dobson, C. M.; Cecchi, C.; Chiti, F. A Causative Link between the Structure of Aberrant Protein Oligomers and Their Toxicity. *Nat. Chem. Biol.* **2010**, *6*, 140−147.
(44) Chiti, F.; Bucciantini, M.; Capanni, C.; Taddei, N.; Dobson, C. M.; Stefani, M. Solution Conditions Can Promote Formation of Either Amyloid Protofilaments or Mature Fibrils from the Hypf N-Terminal Domain. *Protein Sci.* **2001**, *10*, 2541−2547.
(45) Guerrini, L.; Rodriguez-Loureiro, I.; Correa-Duarte, M. A.; Lee, Y. H.; Ling, X. Y.; Garcia de Abajo, F. J.; Alvarez-Puebla, R. A. Chemical Speciation of Heavy Metals by Surface-Enhanced Raman Scattering Spectroscopy: Identification and Quantification of Inorganic- and Methyl-Mercury in Water. *Nanoscale* **2014**, *6*, 8368−8375.
(46) Krpetic, Z.; Guerrini, L.; Larmour, I. A.; Reglinski, J.; Faulds, K.; Graham, D. Importance of Metal−Adsorbate Interactions for the Surface-Enhanced Raman Scattering of Molecules Adsorbed on Plasmonic Nanoparticles. *Small* **2012**, *8*, 707−714.
(47) Turkevich, J.; Stevenson, P. C.; Hillier, J. A Study of the Nucleation and Growth Processes in the Synthesis of Colloidal Gold. *Discuss. Faraday Soc.* **1951**, 55−75.
(48) Frens, G. Controlled Nucleation for Regulation of Particle-Size in Monodisperse Gold Suspensions. *Nature (London), Phys. Sci.* **1973**, *241*, 20−22.
(49) Decher, G. Fuzzy Nanoassemblies: Toward Layered Polymeric Multicomposites. *Science* **1997**, *277*, 1232−1237.
(50) Jeanguillaume, C.; Colliex, C. Spectrum-Image - the Next Step in EELS Digital Acquisition and Processing. *Ultramicroscopy* **1989**, *28*, 252−257.
(51) Arenal, R.; de la Peña, F.; Stéphan, O.; Walls, M.; Tencé, M.; Loiseau, A.; Colliex, C. Extending the Analysis of EELS Spectrum-Imaging Data, from Elemental to Bond Mapping in Complex Nanostructures. *Ultramicroscopy* **2008**, *109*, 32−38.
(52) Spuch-Calvar, M.; Rodriguez-Lorenzo, L.; Morales, M. P.; Alvarez-Puebla, R. A.; Liz-Marzan, L. M. Bifunctional Nanocomposites with Long-Term Stability as SERS Optical Accumulators for Ultrasensitive Analysis. *J. Phys. Chem. C* **2009**, *113*, 3373−3377.
(53) Abalde-Cela, S.; Hermida-Ramon, J. M.; Contreras-Carballada, P.; De Cola, L.; Guerrero-Martinez, A.; Alvarez-Puebla, R. A.; Liz-Marzan, L. M. SERS Chiral Recognition and Quantification of Enantiomers through Cyclodextrin Supramolecular Complexation. *ChemPhysChem* **2011**, *12*, 1529−1535.
(54) Aroca, R. *Surface-Enhanced Vibrational Spectroscopy;* John Wiley & Sons: Chichester, U.K., 2006.

DOI: 10.1021/acsami.5b01056
ACS Appl. Mater. Interfaces 2015, 7, 9420−9428

(55) Michota, A.; Bukowska, J. Surface-Enhanced Raman Scattering (SERS) of 4-Mercaptobenzoic Acid on Silver and Gold Substrates. *J. Raman Spectrosc.* **2003**, *34*, 21−25.
(56) Lee, S. J.; Moskovits, M. Visualizing Chromatographic Separation of Metal Ions on a Surface-Enhanced Raman Active Medium. *Nano Lett.* **2011**, *11*, 145−150.
(57) Ma, W. Q.; Fang, Y.; Hao, G. L.; Wang, W. G. Adsorption Behaviors of 4-Mercaptobenzoic Acid on Silver and Gold Films. *Chin. J. Chem. Phys.* **2010**, *23*, 659−663.
(58) Bishnoi, S. W.; Rozell, C. J.; Levin, C. S.; Gheith, M. K.; Johnson, B. R.; Johnson, D. H.; Halas, N. J. All-Optical Nanoscale pH Meter. *Nano Lett.* **2006**, *6*, 1687−1692.
(59) Chen, L.-M.; Liu, Y.-N. Surface-Enhanced Raman Detection of Melamine on Silver-Nanoparticle-Decorated Silver/Carbon Nanospheres: Effect of Metal Ions. *ACS Appl. Mater. Interfaces* **2011**, *3*, 3091−3096.
(60) Nara, M.; Torii, H.; Tasumi, M. Correlation between the Vibrational Frequencies of the Carboxylate Group and the Types of Its Coordination to a Metal Ion: An Ab Initio Molecular Orbital Study. *J. Phys. Chem.* **1996**, *100*, 19812−19817.
(61) Felgenhauer, K. Protein Size and Cerebrospinal Fluid Composition. *Klin. Wochenschr.* **1974**, *15*, 1158−1164.
(62) Crichton, R. R.; Charloteaux-Wauters, M. Iron Transport and Storage. *Eur. J. Biochem.* **1987**, *164*, 485−506.
(63) Broadley, S. A.; Hartl, F. U. The Role of Molecular Chaperones in Human Misfolding Diseases. *FEBS Lett.* **2009**, *583*, 2647−2653.
(64) Reddy, G. B.; Kumar, P. A.; Kumar, M. S. Chaperone-Like Activity and Hydrophobicity of α-Crystallin. *IUBMB Life* **2006**, *58*, 632−641.
(65) Wang, F. L.; Widejko, R. G.; Yang, Z. Q.; Nguyen, K. T.; Chen, H. Y.; Fernando, L. P.; Christensen, K. A.; Anker, J. N. Surface-Enhanced Raman Scattering Detection of pH with Silica-Encapsulated 4-Mercaptobenzoic Acid-Functionalized Silver Nanoparticles. *Anal. Chem.* **2012**, *84*, 8013−8019.
(66) Arenal, R.; March, K.; Ewels, C. P.; Rocquefelte, X.; Kociak, M.; Loiseau, A.; Stephan, O. Atomic Configuration of Nitrogen-Doped Single-Walled Carbon Nanotubes. *Nano Lett.* **2014**, DOI: 10.1021/nl501645g.
(67) Liu, A. C. Y.; Arenal, R.; Chen, X., Clustering in a Highly Hydrogenated Diamondlike Carbon Determined Using Fluctuation Electron Microscopy and Phenomenological Atomistic Simulations. *Phys. Rev.* **2007**, *76*.
(68) Arenal, R.; De Matteis, L.; Custardoy, L.; Mayoral, A.; Tence, M.; Grazu, V.; De La Fuente, J. M.; Marquina, C.; Ibarra, M. R. Spatially-Resolved EELS Analysis of Antibody Distribution on Biofunctionalized Magnetic Nanoparticles. *ACS Nano* **2013**, *7*, 4006−4013.
(69) Alvarez-Puebla, R.; Liz-Marzan, L. M.; de Abajo, F. J. G. Light Concentration at the Nanometer Scale. *J. Phys. Chem. Lett.* **2010**, *1*, 2428−2434.

DOI: 10.1021/acsami.5b01056
ACS Appl. Mater. Interfaces 2015, 7, 9420−9428